Reports

Smectic Liquid Crystal Monolayers on Graphite Observed by Scanning Tunneling Microscopy

D. P. E. SMITH, H. HÖRBER, CH. GERBER, G. BINNIG

By means of scanning tunneling microscopy, it is observed that molecules of the form *n*-alkylcyanobiphenyl, where *n* = 8 to 12, form two-dimensional crystalline domains when adsorbed onto graphite. The layer spacings measured by tunneling microscopy are 20% larger than those measured previously on bulk material by x-ray diffraction. The structure of the adsorbed molecules is quite different from that of the bulk.

SEVERAL RECENT WORKS HAVE shown that scanning tunneling microscopy (STM) is fulfilling its promise in the understanding of organic and organic-coated surfaces. The studies of tetrathiafulvalene tetracyanoquinodimethane (TTF-TCNQ), a well-ordered conducting molecular crystal (*1*), benzene and CO coadsorbed on Rh (*2*), and smectic and nematic liquid crystals on graphite (*3*) have produced the most unambiguous STM images. These systems all have a high degree of long-range order, making their interpretation relatively simple. The liquid crystal systems studied by Foster and Frommer (*3*) are interesting because of the large number of different molecules that display liquid crystal behavior. This paper presents our results on a series of molecules of the form *n*-alkylcyanobiphenyl (*n*CB), where *n* = 8 to 12, which in bulk form have smectic liquid crystal phases. When deposited on graphite in monolayer quantities, we find that these molecules form two-dimensional crystalline domains whose structure is similar to the bulk smectic phase but is more highly ordered. Moreover, as a result of the interaction with the substrate, the observed structure is a molecular crystal and not a "liquid" crystal. These observations are consistent with the findings of Foster and Frommer (*3*) on 8CB. Two questions left unanswered by the earlier study (*3*) are what is the exact position and orientation of the molecules in the lattice and which molecular orbitals does STM detect. These questions are addressed in this paper.

The samples were prepared by heating a few milligrams of commercially obtained liquid crystal (*4*) to 100°C. Freshly cleaved, highly oriented pyrolytic graphite was placed 2 cm above the heated liquid crystal so that sublimated molecules would condense on the surface. Ellipsometry was used to determine the film thickness. STM images were taken with thicknesses between one and several monolayers. Surprisingly, the STM images were independent of the film thickness. This is consistent with the results of Foster and Frommer (*3*) who deposited a drop of liquid crystal and tunneled through the insulating liquid. This suggests that the STM tip pierces through the uppermost layers and only images the layer in contact with the graphite.

The principles and operation of STM are now well established (*5*). The tunneling microscope used here is similar to the system used in an earlier study (*6*). Tungsten tips were ac-etched in KOH solution and images were formed by monitoring the voltages of a piezoelectric scanner as the tip was scanned over the sample surface at a constant tunnel current of 0.1 nA. Images were taken in air at room temperature. The bias voltage for the images shown here was 0.8 V (tip positive), but varying the voltage between 0.6 and 1.0 V or changing the polarity did not alter the images significantly. It was more important to keep the gap resistance above approximately 5×10^9 ohms, presumably to keep the tip from disturbing the weakly adsorbed layer. If the gap resistance was reduced significantly below this value, the tip would jump abruptly toward the sample and the atomic structure of the graphite substrate would become visible.

Adding a 4-V, 10-μsec pulse to the tunnel gap voltage often dramatically changed the nature of the images, causing an ordered molecular lattice to appear where an atomically flat and featureless surface had been observed before. These pulses possibly removed molecules from the gap or the tip. Another possibility is that when the molecules were deposited onto the substrate they were in an amorphous state. The voltage pulses may provide the energy necessary to fully crystallize the molecular film.

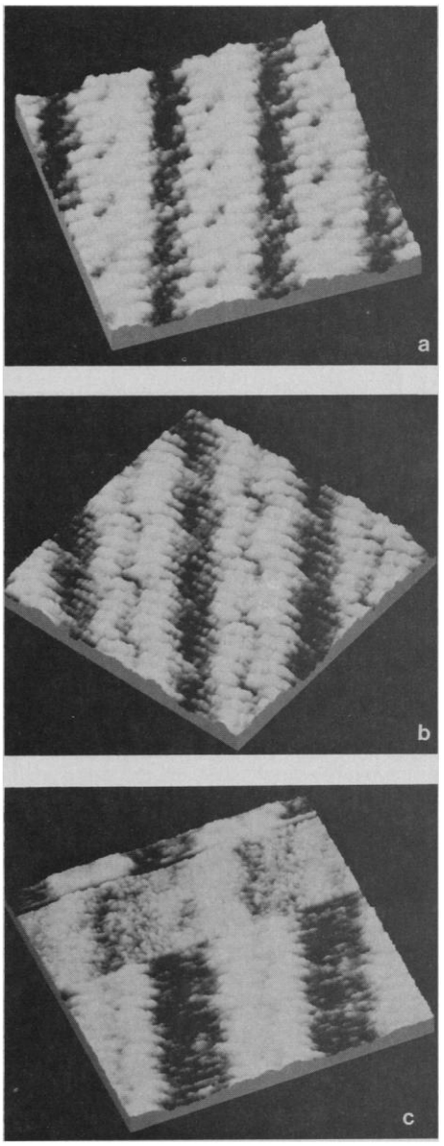

Fig. 1. STM images of cyanobiphenyl molecules absorbed on graphite: (**a**) 8CB, (**b**) 10CB, and (**c**) 12CB. All three images are 114 by 114 Å^2 and were taken at ambient pressure with a tip bias of 0.8 V and tunnel current of 0.1 nA. As the length of the alkyl tail increases, the bright region remains 25 Å wide and the dark region increases in width. In (c) an instability occurred near the top of the image.

Figure 1 shows 114 by 114 Å^2 STM images of 8CB, 10CB, and 12CB taken at 0.8 V and 0.1 nA. The gray scale corresponds to an apparent height range of 1 Å, where white is higher than black (*7*). The images show that 8CB, 10CB, and 12CB form a structure where parallel bright stripes are separated by dark regions. Fine elongated structures with a spacing of approximately 6 Å are seen running nearly perpendicular to the stripes. We interpret each fine structure as a molecule. As the series of image

IBM Physics Group, D-8000 München 40, West Germany.

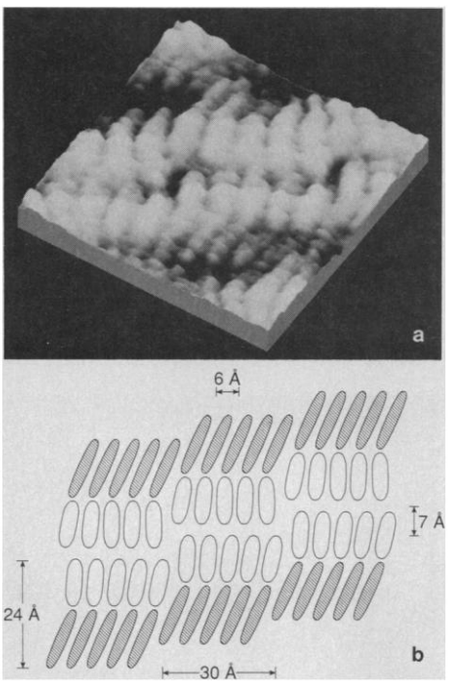

Fig. 2. (**a**) STM image (57 by 57 Å^2) of 10CB on graphite. (**b**) Model showing the packing of the 10CB molecules. The shaded and unshaded segments represent the alkyl tails and the cyanobiphenyl head groups, respectively.

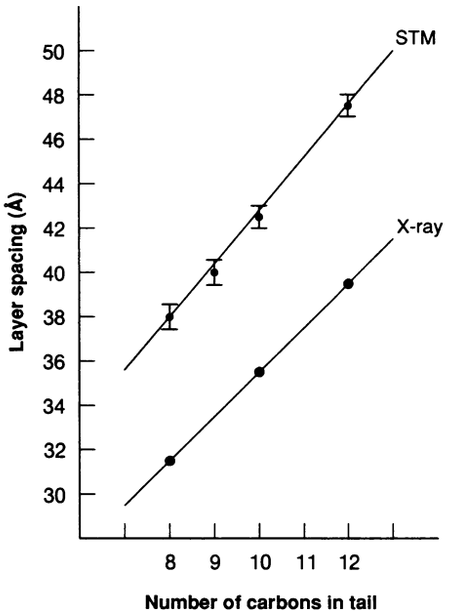

Fig. 3. Smectic layer spacings of cyanobiphenyls versus tail length. The x-ray data is from (*9*) and was performed on bulk liquid crystal material. The error bars represent the standard deviations based on at least ten measurements (STM images) per data point. The source of the error is primarily thermal drifts during measurement.

shows, as the length of the alkyl tail increases, the bright region remains 25 Å wide and the dark region increases in width. This suggests that the bright region corresponds to the cyanobiphenyl head groups of the molecules and the dark region to the alkyl tails. Since each head group is 12 Å long (*8*), the 25 Å width in the STM images implies that two head groups are positioned nearly end-to-end.

The molecular packing is seen more precisely in Fig. 2. This shows a 57 by 57 Å^2 STM image of 10CB and a model of the lattice deduced from the STM images. The model is in agreement with the observed 43 Å lattice spacing. The STM shows that 10CB forms a unit cell with ten molecules arranged into five molecular pairs. The head groups and the tails are slightly interdigitated. The cyano groups try to avoid directly facing each other, presumably because of repulsive electric dipole forces. These forces, perhaps in combination with a possible registry with the graphite substrate, are the probable cause of the noticeable 7 Å lateral shift every five molecular pairs. The 7 Å shift may be a way for the electrostatic energy caused by the proximity of charged cyano groups to be reduced for one-fifth of the molecules. The unit cells of 8CB and 12CB, the other two systems we have examined extensively, are similar to the one shown for 10CB but contain eight molecules arranged in four pairs.

The packing structure of the monolayer films is quite different to the structure of the bulk smectic liquid crystal deduced from x-ray and neutron scattering (*9*) and density measurements (*8*). In the bulk structure it is assumed that the head groups and the tails must fully interdigitate (*8*). Figure 3 shows that the layer spacing (dark region plus light region) of the monolayer films is 1.20 times the bulk smectic layer spacing deduced from x-ray scattering (*9*). This larger layer spacing is the result of the packing structure of the monolayer film in which there is only slight interdigitation of the head groups and tails.

While it might at first seem obvious that the phenyl groups should lie flat on the graphite, this configuration leads to the molecules being spaced at least 6.3 Å apart. The distances we measure between molecules are 6.5 Å for 8CB, 6.0 Å for 10CB, and 5.5 Å for 12CB. The measured molecular spacing for 8CB would allow for the phenyl groups to lie flat but the values for 10CB and 12CB mean that this configuration would cause a very large amount of hydrogen overlap. As a result, we believe that the phenyl groups stand on their sides so that the hydrogens on one side of the carbon rings bond to the graphite and those on the other point normal to the surface. This model has the advantage of suggesting a way for the head groups to bind to the substrate and to reduce the hydrogen overlap between head groups. This structure agrees with the experimental data for 10CB

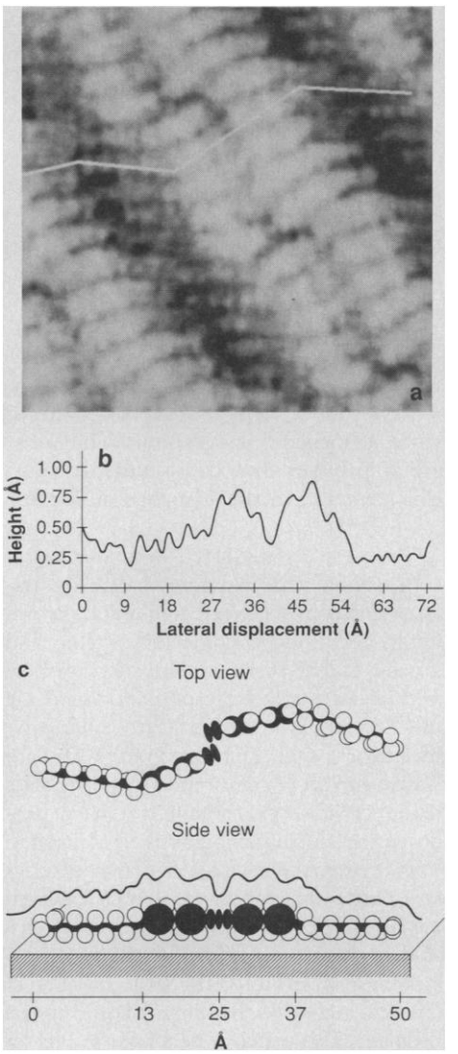

Fig. 4. (**a**) STM image (72 by 72 Å^2) of 10CB. (**b**) Contour line taken along a pair of 10CB molecules. The contour chosen is shown by the white line overlaying the image in (a). (**c**) Model showing the orientation of two molecules of 10CB. A trace is shown representing a possible STM contour.

shown in Fig. 4. (Unfortunately, our data for the other molecules do not have sufficient resolution to determine the orientation of the phenyl groups.) Figure 4, a and b, shows, respectively, an STM image of 10CB and a contour line taken along the conformation of a pair of 10CB molecules. The contour chosen is shown by the white line overlaying the STM image (7). In Fig. 4c we have drawn a model of two molecules of 10CB. The molecule on the left has its alkyl tail oriented so that its carbons alternate up and down. The molecule on the right has the alternate conformation where the carbons alternate side to side. The two possible conformations of the tails explains why in some places the STM detects five spots where the tail should be (half the number of carbons in the tail of 10CB) and in other places the tails are not visible. The model

therefore explains why there is approximately an equal distribution of "visible" and "invisible" tails in the STM images while all the head groups appear the same.

If one takes a simple contour over the vertical component of the hydrogen states in the molecules (Fig. 4c), one obtains a striking agreement with the STM contour in Fig. 4b. Both the 2.5 Å spacing in the alkyl tail and the 3.8 Å spacing in the head group are reproduced. This suggests that the STM is sensitive to the hydrogen orbitals of the molecules. One interpretation is that the contrast in these STM images is due mainly to topography rather than to differences in work function or density of states (*5*); that is, the phenyl groups are "brighter" than the alkyl tails because their hydrogen orbitals are higher above the substrate and have a larger component normal to the substrate. However, it is also possible that the contrast is caused by the perturbation of the graphite wave functions by their interaction with the molecular orbitals. The mixing of the molecular states with the graphite may create new states within 1 V of the fermi energy. Simple (*10*) and extended (*1, 2*) Hückel calculations have been applied quite successfully to STM studies of molecular systems. Such calculations would show more precisely the positions of the empty and filled electronic states of the cyanobiphenyl-graphite system and would help verify the structural model we have proposed.

REFERENCES AND NOTES

1. T. Sleator and R. Tycko, *Phys. Rev. Lett.* **60**, 1418 (1988).
2. H. Ohtani, R. J. Wilson, S. Chiang, C. M. Mate, *ibid.*, p. 2398.
3. J. S. Foster and J. E. Frommer, *Nature* **333**, 542 (1988).
4. BDH Ltd., Poole, England.
5. P. K. Hansma and J. Tersoff, *J. Appl. Phys.* **61**, R1 (1987).
6. D. P. E. Smith *et al.*, *Proc. Nat. Acad. Sci. U.S.A.* **84**, 969 (1987).
7. As with all STM images, the vertical component of the image is sensitive to the tip geometry and the electronic configuration of the tip and sample. As a result, the measured height displacement of the piezoelectric scanner is not an accurate measure of the absolute contours of the molecular adsorbates. Moreover, the observed heights can change depending on the tip condition. See, for example, (*1, 2, 5*).
8. A. J. Leadbetter, J. L. A. Durrant, M. Rugman, *Mol. Cryst. Liq. Cryst.* **34**, 231 (1977).
9. A. J. Leadbetter *et al.*, *J. Physique* **40**, 375 (1979).
10. P. H. Lippel, R. J. Wilson, M. D. Miller, Ch. Wöll, S. Chiang, *Phys. Rev. Lett.* **60**, 2398 (1989).

11. We thank L. Lacomb and M. Niksch for developing image processing software, W. Heckl for performing the ellipsometry measurements, and T. Albrecht, J. Foster, J. Frommer, T. Hänsch, M. Kirk, and J. Spong for very helpful discussions.

24 April 1989; accepted 25 May 1989

Scaling Body Support in Mammals: Limb Posture and Muscle Mechanics

ANDREW A. BIEWENER

The scaling of bone and muscle geometry in mammals suggests that peak stresses (ratio of force to cross-sectional area) acting in these two support elements increase with increasing body size. Observations of stresses acting in the limb bones of different sized mammals during strenuous activity, however, indicate that peak bone stress is independent of size (maintaining a safety factor of between 2 and 4). It appears that similar peak bone stresses and muscle stresses in large and small mammals are achieved primarily by a size-dependent change in locomotor limb posture: small animals run with crouched postures, whereas larger species run more upright. By adopting an upright posture, large animals align their limbs more closely with the ground reaction force, substantially reducing the forces that their muscles must exert (proportional to body mass$^{0.74}$) and hence, the forces that their bones must resist, to counteract joint moments. This change in limb posture to maintain locomotor stresses within safe limits, however, likely limits the maneuverability and accelerative capability of large animals.

BODY SIZE IS ONE OF THE MAJOR factors that affects the form and function of an organism. Because area-dependent functions increase less rapidly than volume-dependent requirements of the organism, severe scaling constraints on functional capacity may result as organisms evolve to larger size (*1*). It has long been recognized that body size is also a critical factor influencing the mechanical support of animals (*2*). Specifically, the ability of muscles to generate force or bones to resist force depends on tissue cross-sectional area, which decreases in proportion to an animal's weight with increased size. Accordingly, considerable emphasis has focused on hypothesized size-dependent changes in the shape of mammalian limb bones (skeletal allometry) (*3*). Yet mammalian limb bones scale surprisingly close to isometry (maintaining similar relative proportions) when considered over nearly the entire size range of the class (*4*). This unexpected finding indicates that stresses acting in the skeleton should increase with increased size. As the material strength of bone does not vary significantly within mammals (*5*), increased locomotor stress would suggest that large animals may operate near to the limit of the strength of their skeletons (a low safety factor). Empirical determinations of skeletal stress in different sized mammals during conditions of strenuous activity (high-speed running or jumping), however, indicate that peak skeletal stresses are fairly uniform for mammals ranging from 0.1 to 300 kg in body mass (*6*), maintaining a safety factor (fracture stress/peak locomotor stress) of between 2 and 4.

To explain these divergent observations, I propose that similar stresses are achieved in the mammalian skeleton by a size-dependent change in locomotor limb posture, shifting from the crouched postures of small animals to the more upright postures of larger species (*7*). Though originally recognized by

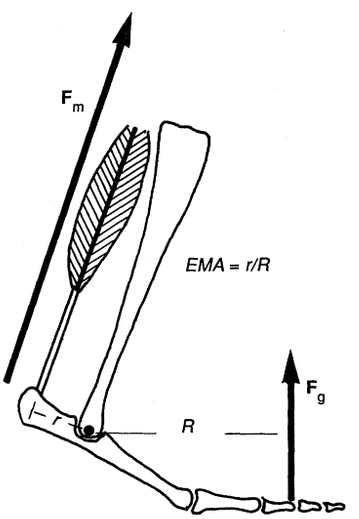

Fig. 1. Schematic illustration of effective mechanical advantage (*EMA*) defined for the extensor muscles acting about the ankle joint. $\mathbf{F_g}$ is the ground reaction force vector (measured with use of a force platform), and R is its mechanical advantage acting about the ankle. $\mathbf{F_m}$ is the force exerted by the ankle extensor muscle group about the ankle with a mechanical advantage of r to counteract the moment exerted by $\mathbf{F_g}$. When muscles had differing mechanical advantages at a joint, a weighted mean mechanical advantage $\bar{r}$ was calculated for the group as a whole (*11*).

Department of Organismal Biology and Anatomy, University of Chicago, 1025 East 57 Street, Chicago, IL 60637.